Chapter 5

Discussion

This chapter is divided into two parts. In the first part, the magnetic structure of the magnetically frustrated regions in thin Mn films is discussed. The focus lies on the comparison between the experimentally observed widening of magnetic frustrations with increasing Mn film thickness and model descriptions of this effect. First, we present a continuum model. In the second approach a Heisenberg model is used.

The second part deals with the discussion of the spin contrast as a function of the bias voltage and theoretical descriptions of this experimental finding. The explanations are based on calculated spin-resolved spectral density of states and current asymmetry calculations. These calculations were performed by J. Henk [118].

5.1 Magnetically frustrated regions

In section 2.1.2, it was shown that a frustration in the magnetic order occurs if an antiferromagnet is in direct contact to a stepped ferromagnetic surface. For the system Cr on Fe(001), the work of Stoeffler and coworkers predicted magnetic defect lines separating two Cr domains above buried Fe step edges. Their calculations showed that the magnetic frustrations are laterally localized in the vicinity of the buried Fe steps and that they widen with increasing Cr thickness [62]. A similar behavior was experimentally observed for the system Mn on Fe(001), as presented in chapter 4. Sp-STM measurements showed spatially localized magnetically frustrated regions at the surface of thin Mn films above buried Fe step edges. These observations suggest that the Mn spins are pinned at the interface by the exchange interaction to the Fe substrate and that the coupling energy at the interface is higher than the domain wall energy in the thin Mn films. This results in magnetic frustrations running through the entire Mn film above an Fe substrate step edge. In the experimental study of Mn films on Fe(001), a liner widening of the magnetically frustrated region which increased in proportion to the Mn film thickness was found. The smallest width of 1.2±0.1 nm was measured between the second and third ML and the largest width of 6.9±0.3 nm between the 18 and 19 ML (±2 ML). The widening of the magnetically frustrated region is a consequence of the pinning of

the Mn magnetic moments at the interface and the tendency to minimize the exchange energy in the frustrated region. Up to the highest Mn thickness investigated, the width of the magnetically frustrated region is increasing and shows no sign of saturation. This indicates that a bulk like arrangement of magnetic moments in the wall will be reached at much higher thickness which cannot be stabilized for this Mn phase. Therefore, the thickness of 20 ML Mn is still too thin to relax the wall width to its bulk value.

5.1.1 Continuum model of the magnetically frustrated regions

In bulk ferromagnets, the width of a 180° domain wall is determined by a competition between the exchange energy and the magnetic anisotropy energy and is given by equation 2.3, in section 2.1. The bulk domain wall width for the cubic itinerant ferromagnets is between 20 and 80 nm [119]. For the layer-wise antiferromagnetic bulk Cr a wall width of about 120 nm [5] has been found. Assuming an antiferromagnetic exchange of similar size and a similar anisotropy, one expects a similar size of a bulk domain wall widths in Mn. By estimating the exchange for Mn (for details see section 5.1.2) and assuming a similar anisotropy as of bulk Fe, a Mn bulk wall width of approximated 20 nm would be expected. Performing a similar approximation by taking the value for the anisotropy for Cr [120], a domain wall width of about 60 nm would result. For the following arguments, the exact knowledge of the bulk domain wall width is not needed. It is only important that it is much larger than the width of the magnetic frustrations measured on the thickest Mn film in our experiments. The linear increase of the magnetic frustration with increasing Mn film thickness supports this argument.

The pinned domain walls in thin Mn layers across buried Fe step edges result in a narrow frustration at the surface between the second and third Mn layer of 1.2 nm. The driving force for the widening of the magnetic frustration for thicker Mn films is the energy which is gained by approaching the bulk domain wall configuration. Thus, the width of the magnetically frustrated region should asymptotically approach its bulk wall width.

Interestingly, we found a slope of the linear increase of the magnetic frustration which is close to 2, meaning that the wall width increases nearly twice as fast as the film thickness. In Fig. 5.1a), the experimental wall width is presented together with the linear function having a slope of 2 (red dotted line).

The slope of 2 of the widening of the magnetically frustrated region can be explained within a continuum model in which the exchange is assumed to be isotropic in any direction. In a similarly frustrated ferromagnet, this would mean that the pinned wall widens isotropically when increasing the distance from the perturbation. Considering a layer-wise antiferromagnet as a ferromagnet where only the magnetization of every second layer is rotated by 180°, a similar homogeneous widening would be expected for the pinned wall in Mn films at Fe steps. In the case of Mn, this

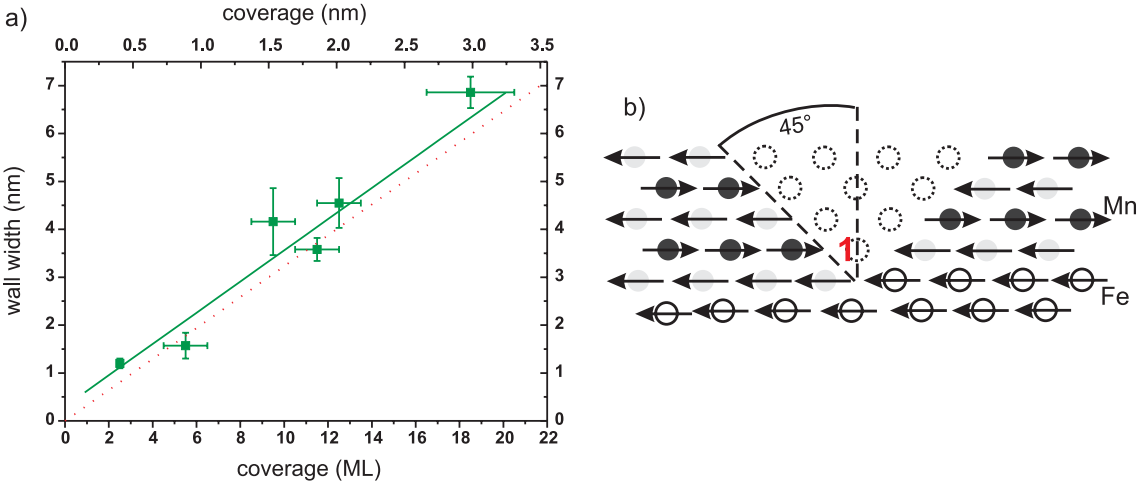

Figure 5.1: The measured data (green data points) with a linear fit (green line) shown in Fig. 4.10 are presented in a) together with a linear function having the slope of twice the film thickness (red dotted line). In b) a schematic sketch of the increase in wall width is presented as expected from simple considerations.

would mean that the ferromagnetic exchange energy within one Mn layer is equal in size to the antiferromagnetic exchange energy to an adjacent Mn layers. The energy needed to turn the magnetization in one point away from its equilibrium state is than only a function of the distance to the neighboring exchange coupled points. This results in a widening of the magnetically frustrated region with an angle of 45°. This corresponds to a linear widening having a slope of twice the film thickness.

Alternatively, this slope can be explained by a simple atomistic bcc model presented in Fig. 5.1b). We again assumed ferromagnetic coupling at the interface between Fe and Mn. Then, the direction of the magnetic moment of atom 1 (see Fig. 5.1b)) placed over the step edge cannot couple ferromagnetically to the Fe atom on the lower right and antiferromagnetically to the Mn atom on the lower left at the same time. The same holds for two Mn atoms in the layer above, for three two layers higher, and so forth which results in an angle of widening of 45°. Again a slope of 2 results.

The linear fit to the experimental data has a slope of 2 but a constant offset occurs to the expected linear function derived by the two models. This may have several reasons. First, the frustrated region in the Mn induces a torque on the Fe moments at the interface via the exchange interaction. This may induce a tilt of the Fe magnetic moments near the step edges. Some of the exchange energy caused by the frustration would then be transferred to the Fe and would widen the magnetic frustration in the Mn film. Second, the Sp-STM has a finite resolution which can lead to a widening in the measured Mn wall profile, especially for narrow walls. A third reason is the limit of the continuum model at the atomic scale. However, this small offset is about the size as the experimental accuracy.

5.1.2 Calculations of the width of magnetically frustrated regions using a Heisenberg model

A different approach which considers the interaction within the exchange coupled system and may provide a quantitative description of the magnetic frustration is a Heisenberg model. The Heisenberg Hamiltonian was introduced in section 2.1. This model is in particular useful due to its simplicity. However, one should keep in mind that localized magnetic moments are considered which is at most a crude approximation for the itinerant magnetic materials like Fe and Mn due to the delocalized nature of the electrons. As shown in Ref. [121], one possibility is to use an effective Heisenberg model to approximate the magnetic interaction in itinerant materials. The itinerant exchange is considered in an effective exchange coupling constant.

To calculate the width of the magnetically frustrated region in the Mn film on Fe(001) an effective Heisenberg model with classical spins is used and in addition, a fourfold magnetic anisotropy is included. The energy of the system can be written as:

$$E = -\frac{1}{2}\sum_{i,j\neq i} J_{ij} cos(\theta_{ij}) + \sum_{i} K_i sin^2\varphi_i cos^2\varphi_i. \tag{5.1}$$

In this notation, the size of the magnetic moment is included in the exchange coupling constant J_{ij}. For the calculations a constant magnetic moment is assumed in each of the two materials (Fe and Mn). $\theta_{i,j}$ is the relative angle between the directions of the magnetic moments i and j. φ_i is the angle between the magnetic moment i and the direction of the easy axis of the Fe substrate magnetic moments, and K_i is the anisotropy constant. This means, only a rotation completely in-plane or out-of-plane is allowed and no difference occurs between these two cases because dipole interactions are neglected. Thus, a Néel wall and a Bloch wall are energetically degenerate[1]. To determine the numerical solution, the angles of the magnetic moments are varied to find the minimum energy configuration.

The values for the exchange coupling constants and the anisotropy constant are well known for bulk bcc Fe. M. Pajda and coworkers [121] calculated J up to the tenth nearest neighbor. The main contributions are given by the nearest and next nearest neighbor, where the next nearest neighbor has still a contribution of 57% of the nearest one. This is mainly due to the bcc structure of Fe where differences of the distance between the nearest and next nearest neighbor are small (about 13%). The other contributions are less than 13% [121].

For bct Mn, the values for J can only be estimated. The value for the nearest neighbor is determined by assuming a linear dependence between the ordering temperature and the exchange coupling constant [121]. The Néel temperature of γ-Mn is $T_N = 540$ K [122,123]. Using this temperature and $J \propto T_N$ a value of $J = -20$ meV is estimated for the nearest neighbor exchange coupling constant. For estimating J

[1] From geometry of a bcc crystalline structure, an antiparallel alignment of all nearest neighbors is possible. Assuming only nearest neighbor interaction, this arrangement is energetically favorable compared to more complex antiferromagnetic order.

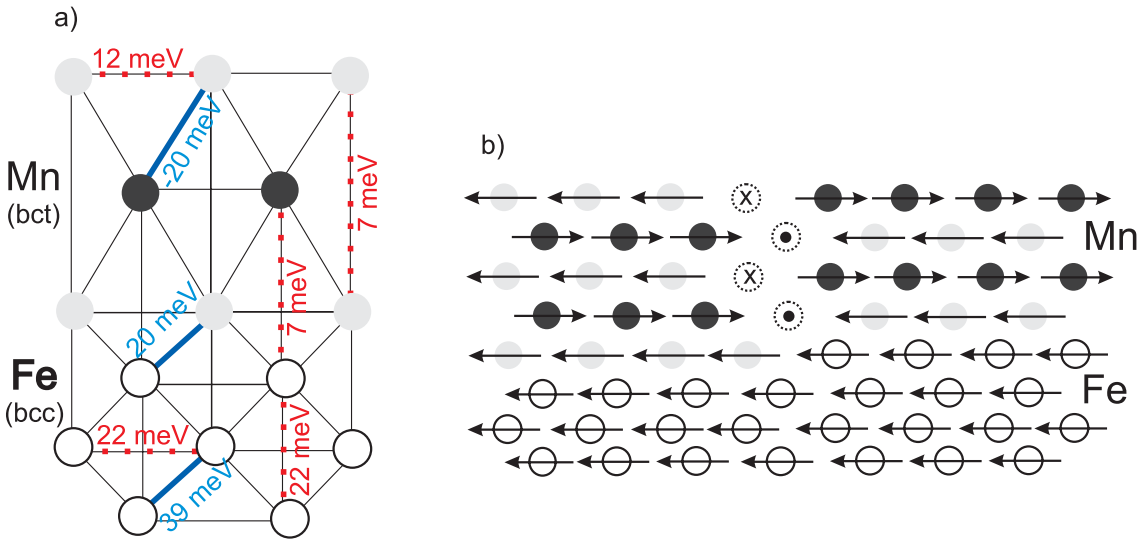

Figure 5.2: The lattice structure of bct Mn on Fe projected in the (100) plane is shown in a). The exchange coupling constants used in the calculations are indicated by numbers. The starting configuration for the calculations in a Heisenberg model is presented in b). The different gray levels of the localized magnetic moments are correlated to the Fe substrate and the layer-wise antiferromagnetic order of the Mn layers. The arrows represent the direction of the magnetic moments parallel or antiparallel to the Fe one and the dots and crosses the moments having an angle of $\pm 90°$.

for the next nearest neighbor exchange in the Mn film, we assumed a decay of the exchange with increasing distance (r) proportional to $\frac{1}{r^5}$. This assumption is based on tight binding calculations [124]. We are aware that this is only a rough estimate but ab-initio calculations of this Mn phase are not available. The calculated values for the nearest and next nearest neighbor exchange for bcc Fe have decay rates between $\frac{1}{r^3}$ and $\frac{1}{r^5}$ [121,125], which supports the assumption. Using this approximation and considering the tetragonal distortion in the Mn film we obtained a next nearest neighbor coupling constant of J =12 meV for the in-plane exchange and J =7 meV for the out-of-plane exchange. The coupling of next nearest neighbors is assumed to be ferromagnetic. At the interface between Fe and Mn the same exchange values are assumed as used in the Mn film.

The choice of the exchange coupling constants is summarized graphically in Fig. 5.2, where the three dimensional structure is projected into a two dimensional plane, for simplicity. The first Mn layer is assumed to couple ferromagnetically to the Fe layer. For the anisotropy the value for bulk Fe was taken (K_i =4 μeV/atom [126]). In the case of thin Mn films, we are in the limit where the magnetically frustrated region is much thinner than a bulk domain wall. While in the latter case, the width is determined by the equilibrium between the exchange and the anisotropy energy, in thin films the width is dominated by the exchange interaction being much higher

than the anisotropy energy. Therefore, the anisotropy in the Mn film can be neglected. To confirm this approximation, test calculations were performed choosing different realistic values for the anisotropy in the Mn film. No changes occurred in the width of the calculated magnetically frustrated region. However, the anisotropy cannot be neglected in the Fe substrate due to the fact that the anisotropy limits the propagation of the magnetically frustrated region into the Fe substrate. In the calculation, the effect of strain or the lattice mismatch in the Mn film at the position of the buried Fe step edge caused by the difference in the out-of-plane lattice constant is not considered.

The starting configuration for the minimization of the energy is presented in Fig. 5.2b). The Fe film is homogeneously magnetized and consists of 70.5 ML. No influence of the magnetically frustrated region was found for thicker Fe films. The thickness of the Mn film is varied between 2.5 and 20.5 ML and an atomically sharp 180° wall is placed above an Fe step edge having the same width in every Mn layer. To check the influence of the starting configuration several different starting arrangements were chosen. For one configuration no magnetic frustration was inserted in the Mn film. The result and especially the calculated width of the magnetically frustrated region was found to be independent of the starting configuration, though the calculation time was significantly increased in some cases. Therefore, the above mentioned starting configuration, which is already close to the energy minimum, was chosen.

Fig. 5.3 shows the result of the calculation of a magnetically frustrated region of 20.5 ML Mn. The result is presented in a two-dimensional plot together with the underlying Fe substrate. Black and white areas correspond to MLs where the magnetic moments have an angle of 180° and 0° compared to the direction of non-tilted Fe magnetic moments. The rotation of the magnetic moments in the magnetically frustrated region is visible and the calculations show that the frustration is localized above the Fe step edge (Fig. 5.3a)). Fig. 5.3b) displays only the Fe film with enhanced contrast (more than 95%) to show the weak tilt of the Fe magnetic moments. The induced rotation of the Fe moments is at most 36° in the top most Fe layer close to the step edge, and it is already reduced to about 7° in a distance of 30 atoms in the plane away from the Fe step edge. In the 10th layer below the step the rotation is reduced to 12°. The size of the rotation of the Fe moments depends strongly on the Mn coverage. For low coverage nearly no rotation is found. From this model, we see that the magnetic frustration in the Mn film induces a torque on the Fe moments due to the exchange which results in a tilt of the Fe moments near the Fe step edge. This means that a topological defect can be associated with a long-range effect extending into the whole antiferromagnetic Mn film and into the ferromagnetic substrate. Calculations performed by Stoeffler and coworkers showed a similar behavior for Cr films overgrowing an Fe step edge [63]. In the calculations, it was found that the magnetic defect line extends into the whole Cr film and that the magnetic moments of the underlying Fe substrate are tilted close to the Fe step edge.

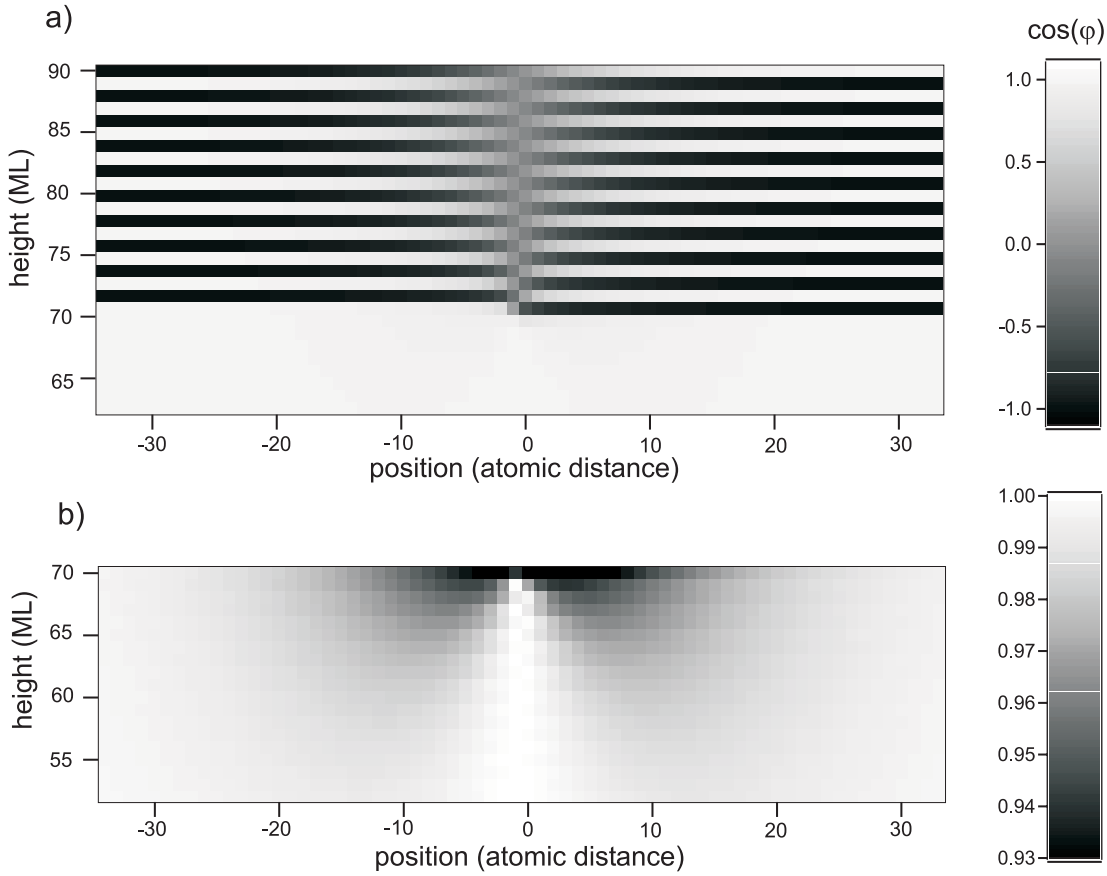

Figure 5.3: a) The calculated angle φ of the local magnetic moments projected along the direction of the undisturbed Fe moments above and below an Fe step edge for a 20.5 ML thick Mn film. The first layers showing the alternating contrast present the antiferromagnetic order of adjacent Mn layers. The Fe magnetic moments below the step edge of a) are shown in b) with a considerably increased contrast (about 95%).

In Fig. 5.4a) a calculated line profile taken at the top most Mn layer in Fig. 5.3a) is shown. To determine the calculated wall width of the magnetically frustrated region, the curve was fitted with a *tanh*-function as in the case of the measured data. A good agreement between the calculated wall profile and the behavior of a *tanh*-function was found (red dots).

Fig.5.4b) shows the width of the magnetically frustrated region within a 20.5 ML thick Mn film from the interface to the Mn surface layer (dashed line). The wall width was determined from line profiles within the film presented in Fig. 5.3. A strong widening is found in the first few Mn layers above the interface and only small changes are found close to the surface layer. In this case, the ratio between the exchange coupling at the interface and in the Mn film is $J_{MnFe}/J_{Mn} = 1$. The product of both, the ratio of J_{MnFe}/J_{Mn} and the film thickness is much bigger than

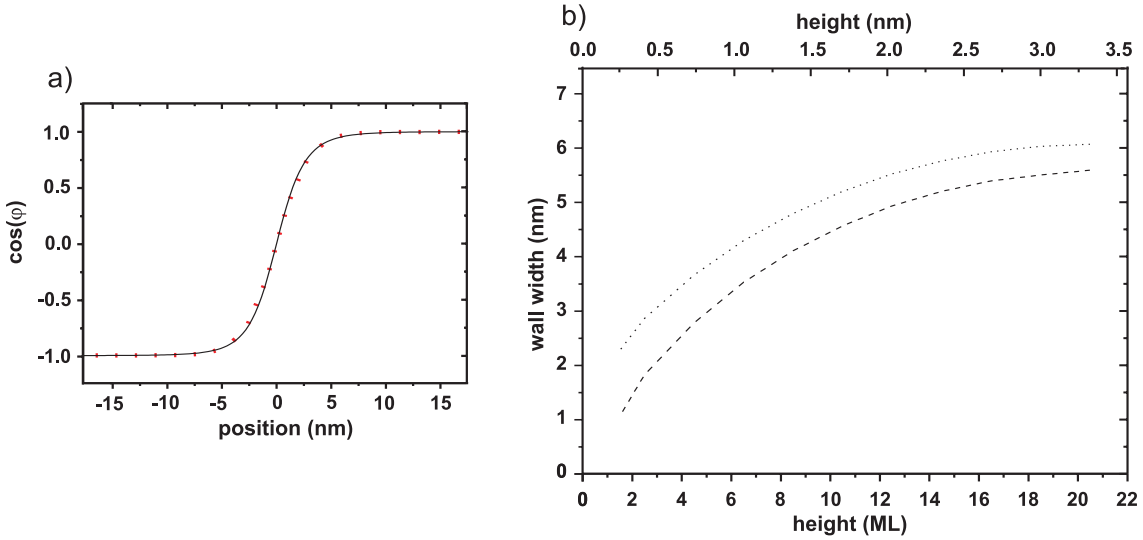

Figure 5.4: a) Calculated line profile projected along the direction of undisturbed Fe moments, taken at the surface of a 20.5 ML thick Mn film (black line) together with a fit of a *tanh*-function (red dots). b) Shows the calculated behavior of a wall within a 20.5 ML thick Mn film for the case that J_{Mn} is equal J_{MnFe} (dashed line) and J_{MnFe} is four times smaller than J_{Mn} (dotted line).

one. For this case, numerical simulations performed by Levchenko and coworkers [59] (for a general system consisting of a thin antiferromagnetic film on top of a ferromagnetic substrate) show a similar behavior of widening of a magnetic frustration within an antiferromagnetic film. In their calculations, a nearest neighbor Heisenberg model was used as a basic model for the simulations. When decreasing the ratio of J_{MnFe}/J_{Mn}, the numerical simulations of Levchenko and coworkers predict that the shape of the curve stays the same and that the curve is only shifted to higher wall width. By decreasing J_{MnFe}/J_{Mn} by a factor four, our calculations yield the curve presented by dots in Fig.5.4b). In agreement with the simulations, the two curves showing nearly the same behavior and the one having a low ratio of J_{MnFe}/J_{Mn} is only shifted to higher wall width.

In Fig. 5.5 the measured wall widths and the calculated widths are shown. Blue stars present the case where the energetic minimum of the magnetic frustrated Mn film was calculated by taking into account only the nearest neighbor exchange interaction. The calculated wall widths as a function of the Mn film thickness have a lower slope than the experimentally determined one and the widths of the walls are smaller. In a next step, the wall width was calculated by considering the nearest and next nearest neighbor exchange interaction. The values of our calculations are indicated by red stars in Fig. 5.5. The slope is much closer to the linear fit to the experimental data, but still a small offset occurs. The calculated width is again smaller than the experimental one. For both calculations a ratio of J_{MnFe}/J_{Mn}=1 was used.

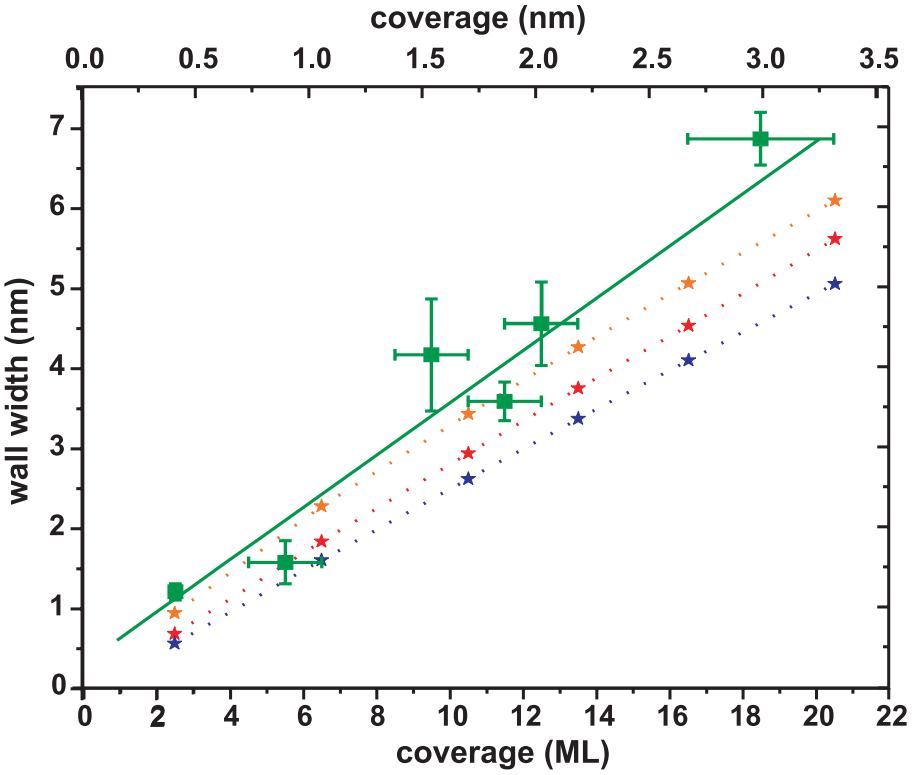

Figure 5.5: The measured data (green data points) with a linear fit (green line) shown in Fig. 4.10 are presented together with the calculated wall widths of the magnetically frustrated region using the Heisenberg model. The calculated data shown in blue are obtained by considering only the nearest neighbor exchange interaction and in red by considering the nearest as well as the next nearest neighbor exchange interaction and the bct structure of Mn. Using the same parameters as in the latter case and reducing the exchange at the interface to 25% one obtains the values presented in orange.

The width of the wall obtained in our calculation with the ratio of $J_{MnFe}/J_{Mn} = \frac{1}{4}$ is presented in orange in Fig. 5.5. The agreement to the experimental data is better than in the case that $J_{MnFe}/J_{Mn} = 1$ (red stars) which suggest that the exchange interaction at the interface between Fe and Mn may be reduced. This prediction is supported by the observation that at some areas no magnetic frustrations were observed at the surface of a Mn film above a buried Fe step indicating a relatively small interface coupling compared to the exchange of Mn (see section 4.2.1). Taking into account the crude approximations in particular for the exchange in the Mn film and at the interface, the agreement between the calculated wall width and the experimental one is rather satisfying.

The remaining difference between the calculated and experimental widths of the magnetically frustrated region may have several origins. The values for the exchange in the Mn film and at the interface are only estimated values. As has been shown, in

particular the exchange interaction at the interface is a critical parameter. Since in the experiment the Mn films were deposited on Fe having a temperature of 370 K, intermixing at the interface occurred which is also not included in the theoretical model. The lattice mismatch (caused by the difference in the out-of-plane lattice constant) at the position where Mn overgrows an Fe step edge is not considered as well. Possible changes of the exchange interaction or of magnetic moments close to the surface and interface are neglected. Several of the above discussed considerations can be taken into account by ab-initio calculations. Therefore, these calculations would be highly desirable for this system.

Both models, the Heisenberg model and the continuum model, describe the widening at the surface rather satisfying. The main difference between these two considerations is the behavior within the Mn film. In the Heisenberg model, a parabolic behavior was found while from the continuum model a linear widening is expected within the Mn film. The behavior within a Mn film is, however, not accessible with Sp-STM measurements.

5.2 Voltage dependent spin contrast

It may be surprising at first glance, that a spin contrast is observed on an antiferromagnetic surface. The basic requirement is the symmetry breaking at the sample surface. In the case of a layer-wise antiferromagnet, each ferromagnetic plane is spin-polarized but adjacent layers have opposite polarization. Therefore, a translation of the crystal by one ML is equivalent to a rotation of the spins by 180°. Due to symmetry reasons, bulk bands in layered antiferromagnets are spin-polarized but degenerate. At the surface, this symmetry is broken resulting in a possible non zero spin contrast at every bias voltages. Using the Sp-STM, this effect should result in a difference in the spin-polarized tunneling current measured between two neighboring Mn layers. Sp-STS studies performed at the surface of a layer-wise antiferromagnetic bulk Cr crystal [5] and Mn films on Fe(001) [6] showed that a spin contrast could be observed only close to spin-polarized surface states.

As we have seen in Fig. 4.13, we find a rather complex dependence of the spin contrast on the bias voltage for ultrathin Mn films on Fe(001) which is difficult to explain only by surface states. Thus, the question arises whether other states can also contribute to a spin polarization on antiferromagnetic surfaces.

Before we address this point, we will discuss the voltage dependent spin contrast measured with the Sp-STM on another antiferromagnetic material, thin Cr films on Fe(001). In this system, the situation seems to be simpler. We have obtained the data by the same technique and under similar conditions as used for the measurements for Mn on Fe(001), for details see section 4.2.2. Cr(001) surfaces show a layer-wise antiferromagnetic order similar to Mn on Fe(001), as illustrated for example by SEMPA (thin Cr films on Fe(001)) [45] and by Sp-STS (bulk Cr(001) single crystal) measurements [5].

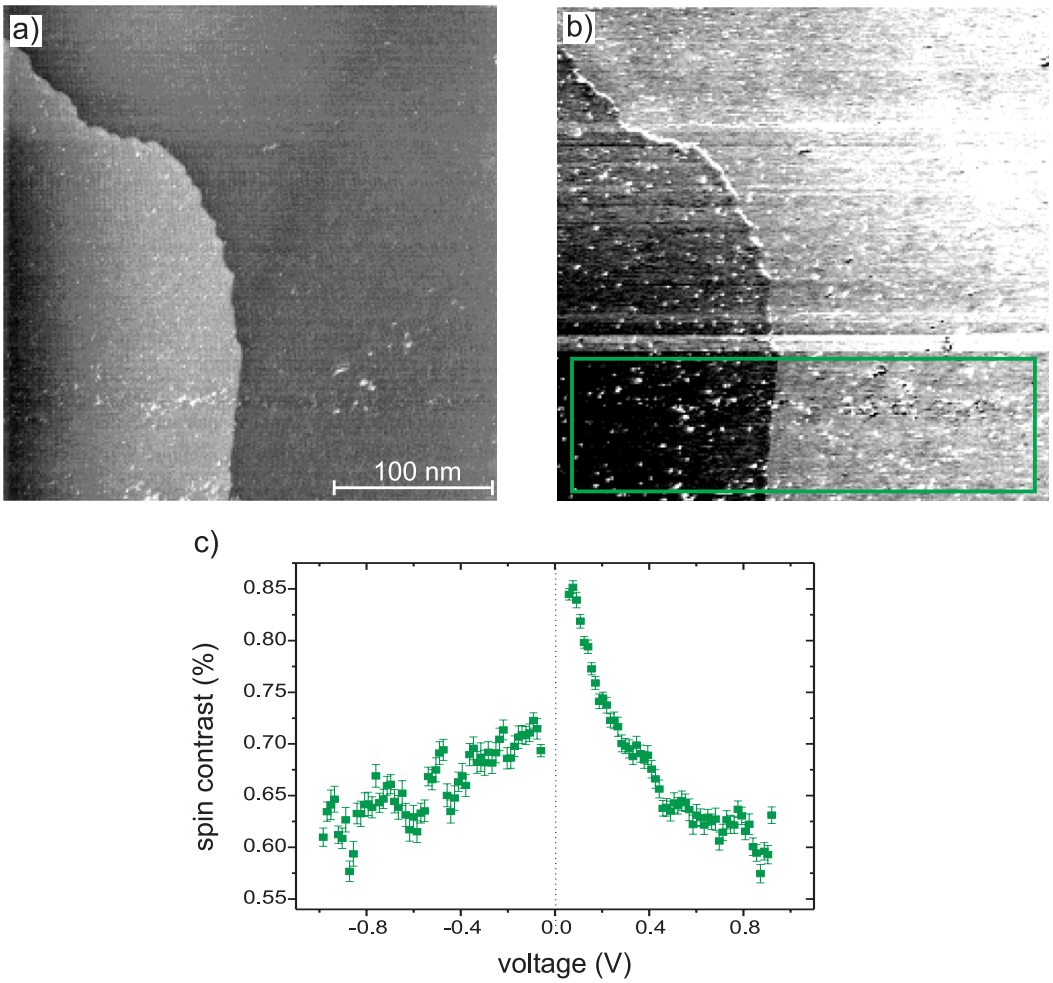

Figure 5.6: a) Topography and b) spin signal of a 12.8 ML thick Cr film on Fe(001). The two different gray levels in a) represent two Cr terraces separated by a monatomic step. The contrast in b) shows the antiferromagnetic order between the two Cr layers. The images were taken at a bias voltage of 0.08 V and an average tunneling current of 3 nA. c) Spin contrast as a function of the bias voltage, obtain within the green box in b). The spin contrast was measured between the 12 and 13 ML (±1 ML) Cr.

An antiferromagnetic order of neighboring Cr layers grown on Fe(001) was imaged with Sp-STM. In Fig. 5.6, a Sp-STM measurement performed on a Cr film of 12.8 ML thickness deposited on Fe(001) at a substrate temperature of about 540 K is presented. In the topography (Fig. 5.6a)), two different Cr terraces are visible which show a different spin polarization in the corresponding spin signal (Fig. 5.6b)). The spin contrast between these two Cr terraces was measured as a function of the bias voltage and the result is shown in Fig. 5.6c). Except for an increase at positive voltages close to 0 V, a constant spin contrast of about 0.6% is observed. As

known from other publications, a surface state exists close to the Fermi level at about −0.05 V [5,85]. Most likely, the increase of the spin contrast is caused by this surface state, which is spin-polarized, as shown e.g. by Sp-STS measurements [5]. Because of the dispersion of the surface state with $k_{\parallel}$, a shift in the energy can occur which may explain the slight shift in the energy position of our measured peak in the spin contrast[2]. In Sp-STS measurements performed on a bulk Cr(001) single crystal [5], a spin signal could only be found close to the spin-polarized surface state. Our observations on Cr films on Fe(001) suggest that the spin contrast measured at voltages different from that of the surface state could be caused by bulk states.

Now we come back to the more complex behavior of the spin contrast with the bias voltage found for Mn films on Fe(001). In this context, a more detailed description of antiferromagnetic bulk bands causing a spin-dependent tunneling current will be given.

To discuss possible underlying physical properties, we describe the relations between our experimental data and the band structure and the spin resolved spectral density of states calculations. Furthermore, the experimental behavior of the spin contrast is compared to calculations of the spin-dependent tunneling current performed for the system Fe(001)/vacuum/Mn/Fe(001) [118].

In general, the theoretical description of the tunneling process is done either in the Tersoff-Hamann or the Landauer-Büttiker approximation, which were introduced in section 2.2. In the Tersoff-Hamann model, only the local density of states at the sample surface at the position of the tip is taken into account. Using this model, a difference in the density of states for spin up and spin down electrons produces a spin-polarized tunneling current.

The calculations of the band structure and the Bloch spectral density of states for bct Mn [118] have been done from first-principles using the local spin-density approximation of the density-functional theory [128]. Here, an appropriate extension of the boundary conditions for surfaces and interfaces was taken into account [129]. The result for $k_{\parallel} = 0$ is presented in Fig. 5.7. The bands in bulk antiferromagnets are degenerate so that the dispersion $E(k)$ for spin up and spin down states is the same, as discussed before. Thus, the depicted bands represent two bands lying on top of each other (Fig. 5.7a)). The spectral density of states is labelled with $+M$ and $-M$ standing for adjacent Mn layers with opposite magnetization (Fig. 5.7b)). The spectral density of states is a local property in real space and thus spin up and spin down electrons show differences depending on the magnetization of the layer. The peaks arising at different energies are only caused by bulk states. No surface states were observed in these spectral density of states [118]. The calculations show that at different energies different spin characters dominate and that the order is reversed in

[2]During this Sp-STM measurement, the distance between the tip and the sample surface was varied as the tunneling current was kept fixed for different bias voltages (see section 4.2.2). Thus, in the range close to 0 V more states with $k_{\parallel} \neq 0$ contributed to the tunneling process in our Sp-STM experiment. The dispersion of surface states is well known for surface states on noble metals [127] and in Mn density of state calculations a similar but weaker effect was found [118].

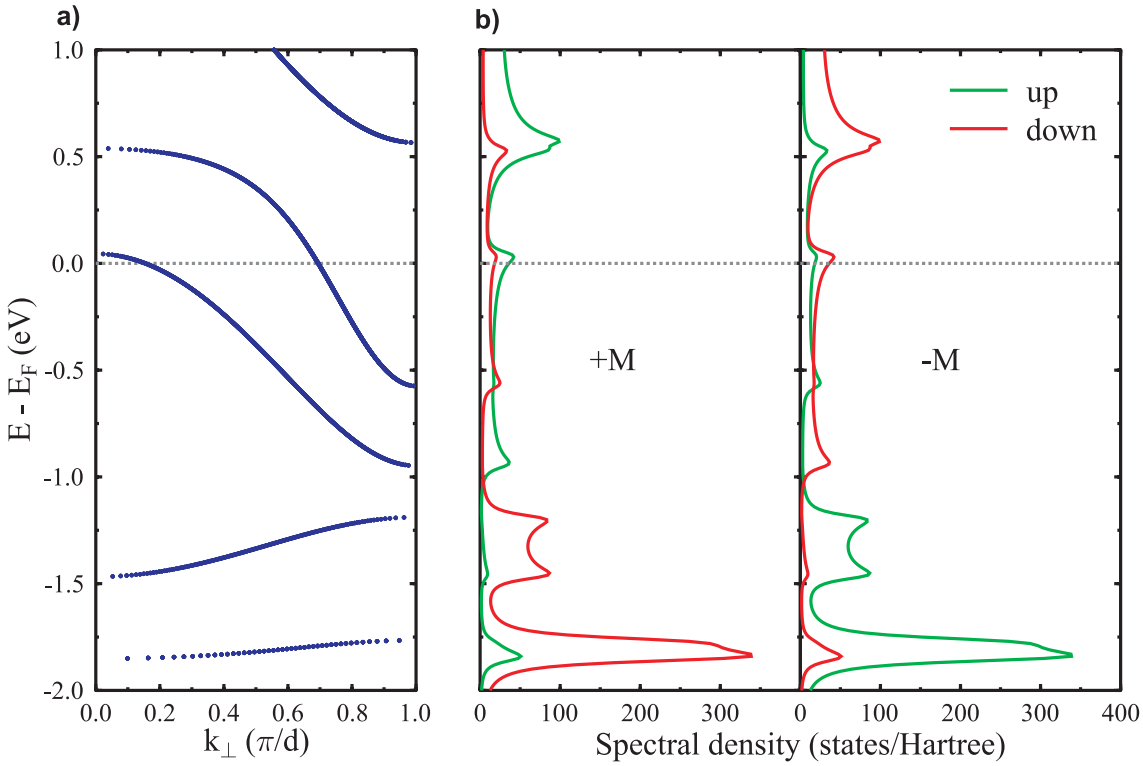

Figure 5.7: a) Result of band structure calculations of a layered antiferromagnetic bct bulk Mn crystal for $k_{\|} = 0$. b) Corresponding spin resolved spectral density for opposite spin-polarized Mn layers indicated by $+M$ and $-M$ [118].

$+M$ and $-M$ layers ($n_{up}(+M) = n_{down}(-M)$). This should result in a spin contrast for certain bias voltages. The experimental data in Fig. 4.13 show a change of sign of the spin contrast for a bias voltage just below 0 V. In the calculations a transition between the spin up and spin down character of the electron states below the Fermi energy is observed. Qualitatively, this change of spin states should produce a change of sign in the spin contrast.

The two shoulders visible in the experimental $(dI/dU)/(I/U)$ spectrum in Fig. 4.14 can be explained on the basis of the band structure and density of states. At the position of both shoulders at about -0.5 V and $+0.25$ V, a band edge is present which creates a small peak in the spectral density. This is most likely responsible for the experimentally measured plateau. The corresponding states of the above mentioned bands have a component perpendicular to the surface. They can contribute to the tunneling current. States of other bands have more contributions in the plane of the surface which results in a reduced transmission probability, like the band being responsible for the high peak at 0.5 V [118].

Another possible approach to describe the measured dependence of the spin contrast as a function of the bias voltage theoretically is a calculation of the current asymmetry based on the Landauer-Büttiker formalism. The current asymmetry δ

is defined as the difference of the tunneling current for parallel (I_P) and antiparallel (I_{AP}) spin alignment of the two electrodes divided by the sum, $\delta = \frac{I_P - I_{AP}}{I_P + I_{AP}}$. I_P and I_{AP} are defined with respect to the direction of magnetization of the underlying Fe substrate. This formalism is a description of the transport in which the transmission probability between the different layers of the whole tunneling system is calculated. Here, realistic band structures are considered and the different matching of the electronic states between the layers is an important quantity for the determination of the tunneling current.

To calculate the spin-polarized tunneling current through thin antiferromagnetic Mn films, the layer-wise order is associated with a periodic arrangement of potential wells and potential barriers, like in a Kronig-Penney model [130]. Thus, an electron of a given spin direction sees an alternating step potential with a period of two ML and an electron of opposite spin is exposed to the same periodic repetition of the potentials but shifted by one ML. Therefore, the transmission of the spin-polarized electrons coming from the spin-polarized underlying Fe substrate is different travelling through an even or odd amount of Mn layers. The ballistic transport calculations of the spin-polarized tunneling current are performed for Mn layers on Fe separated by a vacuum gap from a pure Fe electrode representing the Sp-STM tip. Since in Sp-STM measurements, the tunneling current is determined by states close to the Fermi energy the current asymmetry is calculated for energies between -1 V and +0.6 V. To perform calculations of the current asymmetry using the simplified picture of a Kronig-Penney model, some simplifications of the calculated band structure were done. In this energy range, the Fe bands were approximated by one averaged band which is exchange split. For the antiferromagnetic Mn film the band structure was approximated also by one bulk band where the spin states are degenerate. The potential step in the Kronig-Penney model was chosen in the way to reproduce this band. The result of the current asymmetry is presented in Fig. 5.8a) [118]. The behavior is similar for opposite magnetized Mn layers (here shown for the case of 8 ML and 9 ML Mn) of course with the reversed sign. Above 6 ML Mn, no significant changes of the current asymmetry are expected because no changes are found in the spectral density of states. In Fig. 5.8b), the difference of the current asymmetry between these two oppositely magnetized Mn layers is plotted which represents the experimentally measured situation of the spin contrast.

The main conclusion of this simple model is that the calculated current asymmetry is small, of the order of 1% and changes sign between 0 V and -1 V. These two findings are in qualitative agreement with the experimental results presented in Fig. 4.13. This agreement could only be found when the Fe under the Mn film is considered which provides spin-polarized electrons travelling through the Mn film.

When comparing the experimental data to the ballistic transport theory, a critical parameter is the length that an electron travels before it looses its spin information. If this length is approximately equal to the Mn film thickness, the theory described above, breaks down. In layer-wise antiferromagnets, the spin character of majority and minority electrons alternates with a period of two ML. Thus, this

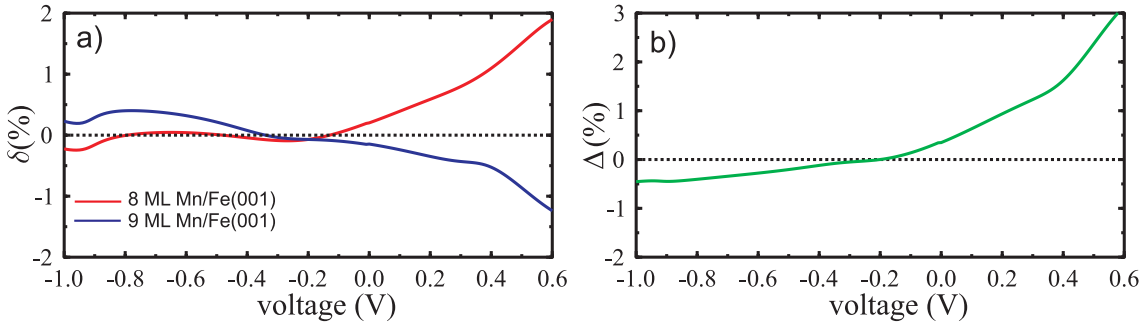

Figure 5.8: a) Calculations of the current asymmetry (δ), the calculations are presented for oppositely magnetized Mn layers, here presented for the case of 8 ML and 9 ML Mn. The difference of the current asymmetry (Δ) between both Mn layers is presented in b) [118].

length will be equal for majority and minority Fe electrons when films of several layers are considered. To the best of our knowledge, this length is unknown for Mn and it is also rather difficult to estimate the value. From literature it is known that the spin diffusion length in Co is about 40 nm [131] near the Fermi edge. This length decreases rapidly when the bias voltage increases. For 1 eV the averaged spin-dependent inelastic mean free path is about 30 Å [132,133]. The inelastic mean free path is, however, smaller than the length that an electron travels before it looses its spin information. Thus, the latter value can be assumed as an upper limit and Mn films under investigation had a thickness of about 20 Å, the theoretical model should be valid.

The calculated data are obtained for $k_{\|} = 0$ and for a constant distance between the Fe electrode and the Mn film surface. Since in the experiment the averaged tunneling current was kept constant while varying the bias voltage, the distance between ring and sample surface changed. This effect is only of importance for small tunneling voltages when the distance is reduced significantly. This might lead to changes in the contribution of states with $\vec{k}_{\|} \neq 0$, which are not considered in the calculations. Thus, the comparison of the experimental data and the calculations is problematic in the range close to 0 V. Hence, the model is not suited to describe the fine details of the experimental data. Considering the simplicity of the model, however, the principal behavior of the measured voltage-dependent spin contrast presented in Fig. 4.13 is in reasonable agreement with the calculated data in Fig. 5.8b). The theoretical model gives a possible explanation of the current asymmetry of thin antiferromagnetic films on a ferromagnetic substrate by considering only the bulk states of Mn. One should keep in mind that localized states, e.g. surface states, do not contribute to the tunneling current in the ballistic Landauer-Büttiker formalism while they will contribute in the Tersoff-Hamann model.

The increase of the measured spin contrast at about 0.1 V can be described on the basis of band structure calculations and spectral density of states. One possible

reason for this experimental finding could be the band edge of one Mn band close to the Fermi edge. Another explanation is based on the contribution of states with different $\vec{k}_{\parallel}$ which have been performed as well, but not presented here [118]. The calculations show that for certain $k_{\parallel}$ a localized resonance is formed at the interface between Fe and Mn and a localized surface state arises in the Mn surface layer at about 0.1 V. Both localized states show the same spin polarization which should lead to a higher transmission from the Fe into the Mn film and from Mn into the vacuum for one spin channel. This enhanced transmission for one spin channel can produce an increase of the measured spin contrast at 0.1 V.

In summery, two different possible theoretical explanations for the spin contrast observed at the Mn surface were introduced. On the one hand, the spin contrast can occur due to the different spin character of bulk Mn states visible in the spin-dependent density of states at the sample surface. On the other hand, the transmission probability of spin-polarized electrons from the underlying Fe could be different for even and odd layers of Mn and it can cause a different spin polarization at the Mn surface.

The calculations show that polarization effects on antiferromagnetic surfaces can arise without any spin-polarized surface states. However, it is likely that the highest spin contrast in both systems, Mn on Fe(001) and Cr on (Fe001), is caused by spin-polarized surface states.